Published in final edited form as:
Soft Matter. 2014 February 7; 10(5): 773–785. doi:10.1039/C3SM52001C.

Inverse Temperature Transition of Elastin Like Motifs in Major Ampullate Dragline Silk: MD Simulations of Short Peptides and NMR Studies of Water Dynamics

Obehi T. Ukpebor[1], **Anup Shah**[2], **Emmanuel Bazov**[2], and **Gregory S. Boutis**[2]
[1]Department of Physics, Hunter College University of New York

[2]Brooklyn College of the City University of New York

Abstract

Using deuterium 2D T_1-T_2 Inverse Laplace Transform (ILT) NMR we have investigated the distribution, population, and dynamics of waters of hydration in major ampullate *N. clavipes* and *A. aurantia* silk as a function of temperature. In both samples studied, correlation times much larger than that of free water are measured and in some cases appear to increase with increasing temperature over the range of 5 to 60 °C(corresponding to reduced tumbling). In addition, the experimental data point to a reduction in the population of water localized in the silk with increasing temperature in the range of 20 to 50°C. Molecular dynamics simulations were performed to probe the thermal characteristics of a variety of repeating motifs found in the two silk samples. The repeating motifs GLGSQ, GAAAAAAG, GPGGY, GPGQQ, GPSG, and GPSGPGS found in *N. clavipes*, GLGSQ, GYGSG, GPGSG, and GPGSQ found in *A. aurantia* silk were found to exhibit a thermal property observed in short elastin peptides known as the "inverse temperature transition". This is a well known characteristic exhibited by short peptides consisting of $(VPGXG)_n$ motifs (where X is any amino acid other than proline) found in elastin, a protein responsible for the elasticity of vertebrate tissues. In qualitative agreement with experimental measurements of water in the silks, all the peptides studied in simulation show evidence of an increase in sidechain contacts and peptide hydrogen bonds, concomitant with a decrease in radius of gyration and localized water as the temperature is raised from approximately 5 to 60° C.

I. INTRODUCTION

Silk is a protein fiber spun by spiders composed of complex protein molecules used for various purposes including capturing prey. Spiders have six or seven sets of glands which produce a distinct silk for a specific function.[1] Orb weaving spiders such as *N. clavipes* and *A. aurantia* are able to synthesize as many as seven different types of silk which include major ampullate, minor ampullate, flagelliform, aggregate, cylindrical, aciniform and piriform silks.[2] Major ampullate silk forms the web framework and is more rigid than the flagelliform, which forms the sticky spiral used for capturing prey, and the cylindrical or tubuliform which forms egg cases. The spinning of silk is a complex process which involves linking a mixture of sticky and nonsticky strands and is controlled by the spinnerets at the tip of the abdomen. Dragline spider silk from the *N. clavipes* and *A. aurantia* contain two proteins: major ampullate spidroin 1 (MaSp1) and major ampullate spidroin 2 (MaSp2).[3–5]

The spider silk which has recently received the most attention is that from the major ampullate gland because of its lightweight characteristics and remarkable mechanical properties.[6] Each protein has unique motifs that control the tensile strength and elasticity that are believed to be responsible for their extraordinary mechanical properties. For

instance MaSp2 has a GPGXX motif, where X can be any one of the small subset amino acids such as serine, tyrosine, leucine, or glutamine. This motif is thought to give the silk elastic characteristics because it is believed to form a β-spiral that is identical to the idealized β-turn of repeating VPGVG motifs present in elastin.[7] One major difference between the two major ampullate proteins is the proline content; there is a large quantity of proline in MaSp2 and little or none in MaSp1.[5] The percentage of MaSp1 to MaSp2 in *N. clavipes* dragline silk is approximately 81:19 while in *A. aurantia* it is approximately 41:59.[8] The ratio between MaSp1 and MaSp2 has been shown to vary between different species of spiders[8] and these differences have been linked to the spider's diet and habitat.[9,10] Table 1 compares the amino acid composition of the major ampullate dragline silk across three different species of spiders and highlights that the glycine and alanine concentrations are relatively abundant while the proline content varies considerably. Gosline and Savage have suggested that the proline concentration may play an important role in silk elasticity[11] as well as the formation of network structures.[12] Optical birefringence studies were performed to probe these effects from the major ampullate silk of *N. clavipes* and *A. diadematus* which have significantly different proline compositions (3.5% for *N. clavipes* and 16% for *A. diadematus*). Their data showed that the birefringence reading recorded for both wet and dry silk of *N. clavipes* is larger than that for the *A. diadematus*, indicating that the network chains in the dry and wet *N. clavipes* silk have stiffer fibers than the *A. diadematus* silk. In *N. clavipes*, glycine and alanine are the most abundant amino acids found in the major ampullate silk and contribute approximately 47% and 26% of the total composition, respectively. The primary structure of the major ampullate dragline silk of *N. clavipes* consists of poly-alanine regions which run up to 7 residues in MaSp1 and 10 in MaSp2 and are believed to form β-sheet like structures.[3,13] In small peptides consisting of $(\text{Ala-Gly-Gly})_{10}$ it was determined that Gly-Gly-X region forms a 3_{10} helix[14–16], and recent experimental studies of *N. clavipes* have confirmed that the gly-rich regions form 3_{10} helix type structures, not disordered helices or random coils.[17]

Work and coworkers[18,19] have shown that when the major ampullate silk from orb weaver spiders comes in contact with water, the silk absorbs water and shrinks by 55% of its original length and subsequently increases its elastic characteristics. This so called "supercontraction" has been linked to specific repeating motifs[20,21] as well as the concentration of proline.[22,23] Vollrath and coworkers showed that the Young's modulus of the major ampullate silks from each species used in the study decreases with increasing proline content. During supercontraction, dragline silk reduces in strength and has properties that resemble an elastomer. Thermoelastic measurements performed by Gosline and coworkers on *A. diadematus* dragline silk immersed in distilled water have shown a reduction in the initial stress of the silk and that its mechanical characteristics are more rubber-like.[24] The signatures of supercontraction have also been observed in *B. mori* silk when the cocoon silk is immersed in a powerful swelling agent[20] and in *A. diadematus* silk when immersed in diferent solvents such as methanol or ethanol.[25] One current belief is that this behavior is linked to the observation that residues such as glycine become more mobile when in contact with a solvent, while repeating alanine motifs which are in β-sheet conformations appear unaffected on the NMR timescale.[20,21,26]

The focus of the present work is to quantify the distribution, population and the dynamical properties of water in *N. clavipes* and *A. aurantia* silks. To study the water dynamics in the silk, we have implemented deuterium 2D T_1-T_2 inverse Laplace transform (ILT) NMR. This experimental method has proven to be powerful for characterizing water in multisite systems and has been recently applied to study the porous properties of water-saturated sedimentary rocks[27], potato tissue[28], cement pastes[29], and to study exchange of water in hydrated elastin.[30] Second, we have used molecular dynamics simulations to investigate the

temperature dependent characteristics of repeating motifs founds in major ampullate *N. clavipes* and *A. aurantia* silks.

II. MATERIALS AND METHODS

A. *Sample Preparation*

Major ampullate dragline silk was collected from adult female *N. clavipes* and *A. aurantia* spiders from central Florida and Arizona, respectively, by winding the silk fiber on a rotating cylinder.[31] During the silking process, the spider was first anesthetized to reduce the stress of capture. The spiders were fed a large cricket once a week, and every other day silk was collected from the major ampullate gland located in the abdomen at a rate of 2 cm/s while being watched closely under a microscope to ensure the silk was not contaminated with minor ampullate silk.

B. *Deuterium T_1-T_2 Correlation Experiments*

All ^{2}H NMR experiments were performed on a Varian Unity 200 MHz spectrometer with a 5 mm liquid probe; the 90° pulse time was tuned to 26 μs. All the silk samples used for these experiments were soaked in D_2O for 24 hours prior to the NMR experiments. During the experiments the samples were suspended in D_2O and the temperature was regulated to within 1°C. The NMR pulse sequence for the T_1-T_2 experiments is illustrated in Figure 1.[32] In the experiments the first 180° pulse inverts the magnetization which recovers toward thermal equilibrium with a relaxation time of T_1 during delay t_1. The second 90° pulse rotates the magnetization into the transverse plane and the NMR signal is detected by a Carr-Purcell-Meiboom-Gill (CPMG) pulse train. We performed measurements by collecting values of t_1 ranging logarithmically from 1 ms to 2 s in 68 steps, using a τ spacing of 300 μs and collecting n=6000 points. The two-dimensional T_1-T_2 NMR relaxation data was processed using an inverse Laplace transform described elsewhere.[33,34]

C. *Molecular Dynamics Simulations*

GROMACS[35] was used in our molecular dynamics (MD) simulations with a Berendsen thermostat[36] and the OPLS-AA/L force field model[37] at six temperatures ranging from 5 to 60°C. Each of the simulations began with a single linear-chain of $[GLGGQ]_5$, $[GLGSQ]_5$, $[GAAAAAAG]_5$, $[GPGGY]_5$, $[GPGQQ]_5$, $[GPSG]_5$, $[GPSGPGS]_5$, $[GYGSG]_5$, $[GPGSG]_5$ and $[GPGSQ]_5$. The peptides were placed in a cubic box measuring approximately 128nm^3 and solvated with 4048 water molecules using the SPC216 water model[38]. The N-terminus of the peptides was terminated using the amine ($-NH_2$) group while the C-terminus was terminated by the carboxyl (-COOH) group. An energy minimization was performed on the structures to remove overlapping atoms. The method of steepest descent was used with the maximum step size set to 1 and the force tolerance set to 2000 kJ/mol nm. We performed a short simulation restraining the peptide positions and equilibrating the pressure for 10 ps before executing the full simulations for a duration of 6 ns. Several properties of the peptides were determined by averaging over the last 1 ns of the simulation results (i.e., from 5 to 6 ns). Figure 2 highlights the averaged Cα Root Mean Square Displacement (RMSD) as a function of time at multiple temperatures for $[GPGSG]_5$ and that after approximately 2 ns equilibrium was established. Similar trends were obtained on all peptides studied.

III. RESULTS AND DISCUSSION

Examples of the acquired T_1-T_2 2D maps at 15 and 50°C for each silk sample studied are shown in Figure 3. The data, shown on a logarithmic scale in intensity, reveal five peaks corresponding to five reservoirs of water with distinguishable dynamical characteristics at low temperature and four peaks at high temperatures for each of the silk samples. An

intriguing observation of the experimental data is that the number of water reservoirs and corresponding relaxation times are remarkably similar in the two silk samples studied.

To verify that the ILT algorithm we implemented can faithfully produce both the intensity and the T_1 and T_2 values that were observed in the experiments, simulations were performed. As an example, taking the *A. aurantia* silk T_1 and T_2 values observed at 15°C, we show simulated data in Figure 4A that was generated with Gaussian distributed noise having a standard deviation in intensity equal to that realized in the experiments. Furthermore, in Figure 4B through 4D results of simulations are provided where the standard deviation of the noise intensity was increased to 5, 7 and 10 times that in our experiments. As shown elsewhere[32], the ILT routine we implemented is prone to producing artifacts in cases where the signal to noise is low. We find that the algorithm fails when the noise was increased to 10 times that in our experiments; the T_1 and T_2 values are not correctly measured and the number of reservoirs is also not correct. However, the figure shows that the ILT is capable at resolving the number of reservoirs, T_1 and T_2 values and relative intensities we observed in the experiments even at 5 times less signal to noise. Similar simulation results were produced for data sets shown in Figure 3, as well as other temperatures that were performed in our study.

Referring again to Figure 3, the two peaks with $T_1 \approx T_2$ in the 2D map have characteristics of isotropic motion in the so-called extreme narrowing limit and denote bulk water and water between the fibers, whereas the peaks closest to the bottom $T_1 > T_2$ exhibit much different dynamics. Additional experiments were performed using a T_2-T_2 correlation experiment[39,40] to probe exchange between the sites resolved in the T_1-T_2 data. Our findings indicated that over time scales from 10μs to 200 ms no exchange was observed. The peaks with $T_1 > T_2$ have characteristics reminiscent of the properties of supercooled heavy water[41] and heavy water in ice[42] where $T_1 > T_2$ was observed. Below, we make the assumption that a complex network of hydrogen bonding occurs between water molecules and between water and the protein surface and analyze the relaxation behavior by the same model used in reference[41].

For a deuterium nucleus in D_2O the deuterium-deuterium dipolar interaction is usually negligible compared with the quadrupolar interaction, and the NMR longitudinal (T_1) and transverse (T_2) relaxation times may be written as follows:

$$\frac{1}{T_1}=\frac{3\pi^2}{20}C^2_{Q_{eff}}\left[2J\left(\omega_0\right)+8J\left(2\omega_0\right)\right] \quad (1)$$

$$\frac{1}{T_2}=\frac{3\pi^2}{20}C^2_{Q_{eff}}\left[3J\left(0\right)+5J\left(\omega_0\right)+2J\left(2\omega_0\right)\right]. \quad (2)$$

In the above expressions ω_0 is the Larmor frequency of the deuterium nucleus, $C_{Q_{eff}}=\frac{e^2q_{eff}Q}{h}\Gamma$. The model in the formulation above assumes that the motion of the water molecule may be divided into fast oscillatory motions and slower diffusional processes[41]. Following Lang et. al., the short time reorientational motions of any given water molecule consists of fast librations about an equilibrium orientation in a random network of surrounding water - in our system the network would also include protein molecules. On a much longer time scale, the orientation of the water molecule will change due to diffusive motion resulting in a rearrangement of the surrounding network of water as well as protein molecules. The librational motion in this model is tacitly assumed to occur at a much shorter time scale than the diffusive motion, and as a consequence the cross-correlation between the

two relaxation pathways is assumed to be negligible. The spectral density in these expressions is defined by $J(m\omega_o) = \frac{\tau_c}{1+(m\omega\tau_c)^2}$, with τ_c denoting the slow diffusion correlation time of the water molecule. As shown in[43] the autocorrelation function characterizing the slow and fast motions may be separated, resulting in the expressions for T_1 and T_2 above. The motional averaging parameter Γ in $C_{Q_{eff}}$ is given by

$$\Gamma = \sum_m |<D^{(2)}_{om}(\Omega_{IF})> + \frac{\eta}{\sqrt{(6)}}\left[<D^{(2)}_{-2m}(\Omega_{IF})> + <D^{(2)}_{2m}(\Omega_{IF})>\right]|^2. \quad (3)$$

In the above expression the terms $D(\Omega)$ denote second rank Wigner rotation matrices, and the subscript IF refers to a transformation from the principle axis (I) of the field gradient tensor to the equilibrium orientation of the oxygen-deuterium bond(F)[41]. The parameter $\eta = (V_{xx} - V_{yy})/V_{zz}$ is the asymmetry parameter of the potential V. For deuterium in bulk water the asymmetry parameter η is approximately zero, however exact knowledge of η is not necessary for determining the correlation time τ_c and constant $C_{Q_{eff}}$.

Using Eq. 1 and Eq. 2 we have determined the correlation times and values of $C_{Q_{eff}}$ as a function of temperature, and have tabulated our findings in Tables 9-10. The correlation times for the peaks with $T_1 > T_2$ are significantly higher than that of free water, which is approximately 5 ps at room temperature. In addition, in both of the silk samples studied (refer to Tables 9-10) two of the three water reservoirs exhibit correlation times that increase with increasing temperature over the range studied. In addition, Figure 4 shows the relative population of these peaks (where $T_1 > T_2$) to the total signal intensity observed in the 2D map at every temperature (the population was determined by integrating the signal areas in the 2D maps). The figure indicates that the percentage contribution of the waters of hydration with ($T_1 > T_2$) reduce in intensity with increasing temperature.

Dielectric relaxation methods have been recently used to investigate water in restricted environments, such as micelles and microemulsions, and have shown that bulk water experiences fast solvation dynamics at picosecond timescales while confined water may experience slow nanosecond solvation dynamics.[44–46] The origin of the slow dynamics in this, and in many other systems such as lipids[47] and DNA molecules[48], is currently under debate in the community. Nevertheless, molecular dynamics simulations of water in simplified geometries, for example, have revealed a slowing down of solvation dynamics upon confinement.[49,50] These results are reminiscent of what we have experimentally observed in the hydrated silk of *N. clavipes* and *A. aurantia* where the tumbling correlation times of water with $T_1 > T_2$ range from 5 to 35 ns. Interestingly, similar values for the correlation times have been observed in experimental studies of water in elastin.[51]

The static quadrupolar coupling constant $\frac{eq_{zz}Q}{h}$ for deuterium in heavy water at room temperature is approximately 214 kHz[41]. In the *N. clavipes* and *A. aurantia* silk samples we found that $4\pi^2 C^2_{Q_{eff}}$ ranged from approximately $1 \times 10^{10}[s^{-2}]$ to $10 \times 10^{10}[s^{-2}]$, thus $C_{Q_{eff}}$ ranges from approximately 10 to 50 kHz. This effective quadrupolar coupling constant is different than the static or instantaneous value and includes librational motion parametrized by Γ defined by equation 3. The constant $C_{Q_{eff}}$ appears to vary for some of the components as a function of temperature, which may be a result of the thermally induced changes in the density of water within each reservoir, or the extent of hydrogen bonding between water molecules and water molecules and silk. Simulation studies have shown that the quadrupolar coupling constant reduces by approximately 30% from its static value and the asymmetry parameter η by increases %20 when the O-D bond length in heavy water changes by only %6[42]. However, the differences observed in the static quadrupolar coupling constant and

that measured in the water in silk would suggest a larger difference, which may include variations in the O-D bond length as well as anisotropic motion that was not included in the formulation of the model for equations 1 and 2. The observation of a reduced quadrupolar coupling constant on the order of 120 kHz in D_20 has been reported in recent work of structural water in helical peptides[52].

Tables 2 and 3 highlight the known primary structures for *N. clavipes* and *A. aurantia* silks. Glycine and alanine make up the majority of the composition any one of the samples, and one point to take note of is the similarity in the repeating motifs found in each silk. *N. clavipes* and *A. aurantia* major ampullate silks are made up of similar repetitions such as GLGSQ, GYGGQ, GPSG and GPGQQ. Additionally, there are blocks of alanine regions in the spider silks which form β-sheets which would be expected to not allow for the penetration of water.[53] Results from the molecular dynamics simulations of the peptides studied in this work are tabulated in Table 4 through Table 8. The general trends in all of the simulations we performed point to an increase in sidechain contacts and peptide hydrogen bonds, concomitant with a decrease in the number of peptide-water hydrogen bonds, radii of gyration, solvent accessible surface areas (SASA)s, non-polar SASAs and number of proximal water molecules as the temperature is raised from 5 to 60°C. This finding is reminiscent of an observation made in simulation based studies of short elastin mimetic peptides VPGVG and LGGVG.[54] One peculiarity in our experimental data, shown in Figure 4, is that the population of water decreases from 20 to 25 °C, but then increases slightly when the temperature is raised to 30 °C and additional heating of the samples results in further reduction of the population of water with $T_1 > T_2$. Some of the peptides we simulated also exhibit this characteristic near 35 °C; for example the repeating motifs $(GYGSG)_5$,$(GLGSQ)_5$, $(GLGGQ)_5$, and $(GPGGY)_5$ show a clear decrease in the number of proximal water molecules as the temperature is raised from 5 to 25 °C, however at 30 °C the number of water molecules within 0.6nm of the peptide atoms increases, and additional heating of the peptide to 60 °C results in further expulsion of water.

Examples of the Ramachandran maps from our simulations for the various motifs we investigated are shown in Figure 6. The figures were produced by accounting for the dihedral angles in the last 1 ns of any given simulation. In each figure we have normalized the integrated Ramachandran space to unity so that the results across temperatures may be compared. Overall, we find that the general features in any of the Ramachandran maps are that the motifs occupy a larger region of the dihedral space at 60°C compared with 5°C. This general feature appears to be reminiscent of the simulation findings of the elastin mimetic peptide $(VPGVG)_{18}$[55]. To our knowledge NMR experiments on hydrated *N. clavipes* or *A. aurantia* have been performed only at or near 25°C, however there is good agreement between these experimental results and our short time simulations which we discuss below.

Referring to Figure 6, at 25°C the dihedral angles $(\Phi, \Psi)=(150,-80)$ and $(-150,150)$ in the alanine motifs in $(GAAAAAAG)_5$ which appears in *N. clavipes* reveals the strong presence of β-sheet motifs. The observation of β sheet structural features in the repeating alanine segments of this silk is well known in both hydrated[3] and dry silk samples[56]. Our simulations also appear to indicate a very small population of structures that occupied the region of space near $(\Phi, \Psi)=(-80,-20)$ which would appear to be α-helical. Experiments on a short MaSp1 *N. clavipes* peptide which include the motif -GAAAAAAG- have shown that the alanine in close proximity to glycine adopted an α-helical structure when exposed to various solvents[57]. Additionally, experiments performed on ^{13}C labeled silk from *N. edulis* revealed that approximately seventy-three percent of all the torsion angles for alanine motifs occupied the β-sheet region, with the remainder being α-helical[58]. Referring again to Figure 6, our simulations indicate that leucine in the repeating motif $(GLGGQ)_5$ shows a large population in the dihedral range near $(\Phi, \Psi)=(-90,120)$ which we interpret to be a distorted

3_1 helix at 25°C; this finding is in agreement with recently reported experimental work performed by J. Ashida and coworkers on short model peptides consisting of AGG and LGG motifs[59]. In recent simulation studies of MaSp1 and MaSp2 proteins from the *N. clavipes* spider dragline silk the proline motifs were observed to take up type I and type II β-turn conformations with a small α-helical component[60]. Our results presented in Figure 6 for the proline residues in $(GPGQQ)_5$ agree well with these findings, and experiments on $^{13}C/^{15}N$-proline labeled *A. aurantia* dragline silk which provide evidence for an elastin-like β-turn structure for the repetitive Gly-Pro-Gly-X-X motif prevalent in major ampullate spidroin 2 (MaSp2)[61]. Lastly, we show examples of the Ramachandran maps for the tyrosine residues in $(GPGGY)_5$ at 5°C, 25°C and 60°C. The simulations at 25°C indicate what may be interpreted as either a 3_1-helix or type II β-turn in addition to an almost equal population of an α-helical motif. In experiments on uniformly ^{13}C labeled hydrated *N. clavipes*, tyrosine exhibited random coil characteristics on the NMR time scale[3]. The distribution of dihedral angles taken up by tyrosine in $(GPGGY)_5$ in our short time simulations may account for this observation. To experimentally probe the structural changes with temperature is beyond the scope of the present work, however, we believe that studies on short peptides using well known two dimensional NMR methodology, such as a spin diffusion experiment, should be feasible (see reference[57] for example).

Gosline and coworkers reported on an experimental measurement of the relative length versus temperature on major ampullate silk of *A. diadematus* between 10 and ~30°C suspended in distilled water[24,62]. Their results showed a decrease in the initial length of the silk with increasing temperature from 10 to 30°C. Over this temperature range, the linear coefficient of expansion was found to be $-1.8\times10^{-4}°C^{-1}$ and above 30°C the linear coefficient was observed to markedly change to $-3.9\times10^{-4}°C^{-1}$. The observed negative thermal expansion coefficient correlates well with what we observe in our simulations of short silk motifs and in our experimental studies of water in the silk samples. During supercontraction, the expulsion of water and reduction in size should be interpreted as entropic in origin; increase in temperature results in an further increase in configurational entropy. The change in configurational entropy in hydrated silks allows for rubber-like characteristics-hydrated silk elasticity is driven by an entropic force (F_{Ent}=-T∂S/∂L) familiar in the classical treatment of rubber elasticity.

D.W. Urry and coworkers have experimentally demonstrated the so-called “inverse temperature transition” in an elastin polypentapeptide $[VPGVG]_n$.[63] In one study, by measuring the carbonyl ^{13}C NMR relaxation times as a function of temperature, a transition in the mobility of the backbone was observed; the experimental data showed an increase in mobility of the protein upon raising the temperature between 10 to 25°C, then a reduction in mobility was observed from 25 to 40°C. The simulation studies of V. Daggett and coworkers on the elastin mimetic peptide[55] $[VPGVG]_{18}$ have given further insights into the inverse temperature transition of this peptide. Similar to the findings reported in this work, their simulations showed an increase in protein hydrogen bonds and side-chain contacts, as well as a decrease in SASA, radius of gyration, and number of localized water molecules as the temperature is raised from 5 to 60°C. The unique thermal behavior of short elastin peptides, usually having the repeat $[VPGXG]_n$ (where X is any amino acid except proline), has recently gained interest for a wide range of applications. In drug delivery, for example, elastin based peptides have been used to target a tumor site due to the fact that these peptides undergo an inverse temperature transition which is sensitive to pH and/or temperature[64]. Chilkoti and others[65–70] have used modified elastin like peptides as drug carriers to the sites where tumors are located; in one study involving a mouse model[71], it was found that this method of drug delivery slows down the progression of the tumor significantly. Additionally, elastin like peptides that exhibit an inverse temperature transition are currently at the heart of many research endeavors relating to tissue engineering[72] for suture and

cartilage repairs, and in other biotechnology applications[73,74]. Our simulation findings indicate that many motifs found in silks exhibit thermal characteristics similar to the well studied VPGVG motif of elastin and may be of use in these and other applications.

IV. CONCLUSION

In this work we have reported on measurements of the relaxation times of water hydrated *N. clavipes* and *A. aurantia* silks as a function of temperature by deuterium 2D T_1-T_2 ILT NMR. This experimental approach was used to enumerate the number of water reservoirs observable on the NMR time scale and to characterize their relative populations, and dynamics. In all of the silk samples studied we observed the most restricted components of water (where $T_1 > T_2$) reducing in population with increasing temperature between 20°C and 50°C. These components of water had correlation times much larger than that of free water, suggesting restricted and/or anisotropic dynamics. While the experimental method has allowed for distinguishing the number of water reservoirs based on their dynamical characteristics, this approach does not allow one to establish their location in proximity to any structural motifs of the silk. Molecular dynamics simulations were performed to probe the thermal characteristics of a variety of repeating motifs found in *N. clavipes* and *A. aurantia* silks. In simulations, we find that the peptides exhibit characteristics reminiscent of the so-called inverse temperature transition found in short elastin like motifs as the temperature is raised from 5°C to 60°C. In $[GLGGQ]_5$, $[GLGSQ]_5$, $[GAAAAAAG]_5$, $[GPGGY]_5$, $[GPGQQ]_5$, $[GPSG]_5$, $[GPSGPGS]_5$, $[GYGSG]_5$, $[GPGSG]_5$ and $[GPGSQ]_5$ peptides, we observed a decrease in the radius of gyration, SASA, non-polar SASA as well as an increase in the number of side-chain contacts and the number of peptide-peptide hydrogen bonds as the temperature is raised from 5 to 60°C. In addition, the simulations also reveal a decrease in number of water molecules similar to what was observed in the experimental measurements using 2D T_1-T_2 ILT NMR methodology.

Acknowledgments

This research was supported, in part, by a grant of computer time from the City University of New York High Performance Computing Center under NSF Grants CNS-0855217, CNS-0958379 and ACI-1126113. G.S. Boutis acknowledges support from award No. SC1GM086268-06 from the National Institute of General Medical Sciences and funding from the PSC-CUNY. The content is solely the responsibility of the authors and does not necessarily represent the official views of the National Institute of General Medical Sciences or the National Institutes of Health (NIH). O. T. Ukpebor acknowledges supported from the RISE program at Hunter College under Grant GM060665. The authors thank Gregory P. Holland for providing the *N. clavipes* and *A. aurantia* dragline silk samples and Tetsuo Asakura for useful discussions. In addition we thank Moshe C. Silverstein, Steven Morgan and Anthony Papaioannou for useful discussions and help with the simulations and Yi-Qiao Song for the use of the ILT code. Lastly we thank Noel Goddard for useful comments relating to this work.

REFERENCES

1. Murad AM, Rech EL. Journal of Molecular Modeling. 2010; 17:1183–1189. [PubMed: 20697759]
2. Hinman MB, Jones JA, Lewis RV. Trends in Biotechnology. 2000; 18:374–379. [PubMed: 10942961]
3. Holland GP, Jenkins JE, Creager MS, Lewis RV, Yarger JL. Biomacromolecules. 2008; 9:651–657. [PubMed: 18171016]
4. Xu M, Lewis RV. Proceedings of the National Academy of Sciences. 1990; 87:7120–7124.
5. Hinman MB, Lewis RV. Journal of Biological Chemistry. 1992; 267:19320–19324. [PubMed: 1527052]
6. Gosline J, Guerette P, Ortlepp C, Savage K. Journal of Experimental Biology. 1999; 202:3295–3303. [PubMed: 10562512]
7. Urry DW, Ohnishi T, Long MM, Mitchell LW. International Journal of Peptide and Protein Research. 1975; 7:367–378. [PubMed: 1184287]

8. Brooks AE, Steinkraus HB, Nelson SR, Lewis RV. Biomacromolecules. 2005; 6:3095–3099. [PubMed: 16283732]
9. Craig CL, Riekel C, Herberstein ME, Weber RS, Kaplan D, Pierce NE. Molecular Biology and Evolution. 2000; 17:1904–1913. [PubMed: 11110907]
10. Tso I-M, Wu H-C, Hwang I-R. Journal of Experimental Biology. 2005; 208:1053–1061. [PubMed: 15767307]
11. Hayashi CY, Shipley NH, Lewis RV. International Journal of Biological Macromolecules. 1999; 24:271–275. [PubMed: 10342774]
12. Savage KN, Gosline JM. Journal of Experimental Biology. 2008; 211:1937–1947. [PubMed: 18515724]
13. Simmons A, Ray E, Jelinski LW. Macromolecules. 1994; 27:5235–5237.
14. Ashida J, Ohgo K, Komatsu K, Kubota A, Asakura T. Journal of Biomolecular NMR. 2003; 25:91–103. [PubMed: 12652118]
15. Holland GP, Creager MS, Jenkins JE, Lewis RV, Yarger JL. Journal of the American Chemical Society. 2008; 130:9871–9877. [PubMed: 18593157]
16. van Beek JD, Hess S, Vollrath F, Meier BH. Proceedings of the National Academy of Sciences. 2002; 99:10266–10271.
17. Bratzel G, Buehler MJ. Journal of the Mechanical Behavior of Biomedical Materials. 2012; 7:30–40. [PubMed: 22340682]
18. Work RW. Journal of Experimental Biology. 1985; 118:379–404.
19. Work RW. Journal of Arachnology. 1981; 9:299–308.
20. Yang Z, Liivak O, Seidel A, LaVerde G, Zax DB, Jelinski LW. Journal of the American Chemical Society. 2000; 122:9019–9025.
21. Jelinski LW, Blye A, Liivak O, Michal C, LaVerde G, Seidel A, Shah N, Yang Z. International Journal of Biological Macromolecules. 1999; 24:197–201. [PubMed: 10342765]
22. Creager MS, Jenkins JE, Thagard-Yeaman LA, Brooks AE, Jones JA, Lewis RV, Holland GP, Yarger JL. Biomacromolecules. 2010; 11:2039–2043. [PubMed: 20593757]
23. Liu Y, Sponner A, Porter D, Vollrath F. Biomacromolecules. 2008; 9:116–121. [PubMed: 18052126]
24. Gosline JM, Denny MW, DeMont EM. Nature. 1984; 309:551–552.
25. Shao Z, Young RJ, Vollrath F. International Journal of Biological Macromolecules. 1999; 24:295–300. [PubMed: 10342778]
26. Holland GP, Lewis RV, Yarger JL. Journal of the American Chemical Society. 2004; 126:5867–5872. [PubMed: 15125679]
27. Kleinberg R, Farooqui S, Horsfield M. Journal of Colloid and Interface Science. 1993; 158:195–198.
28. Hills B, Costa A, Marigheto N, Wright K. Applied Magnetic Resonance. 2005; 28:13–27.
29. McDonald PJ, Korb J-P, Mitchell J, Monteilhet L. Physical Review E. 2005; 72:011409.
30. Sun C, Boutis GS. New Journal of Physics. 2011; 13:025026.
31. Work RW, Emerson PD. Journal of Arachnology. 1982; 10:1–10.
32. Song Y-Q, Venkataramanan L, Hurlimann M, Flaum M, Frulla P, Straley C. Journal of Magnetic Resonance. 2002; 154:261–268. [PubMed: 11846583]
33. Venkataramanan L, Song Y-Q, Hurlimann MD. IEEE Transactions on Signal Processing. 2002; 50:1017–1026.
34. Neudert O, Stapf S, Mattea C. Journal of Magnetic Resonance. 2011; 208:256–261. [PubMed: 21185207]
35. Hess B, Kutzner C, van der Spoel D, Lindahl E. Journal of Chemical Theory and Computation. 2008; 4:435–447.
36. Berendsen HJC, Postma JPM, van Gunsteren WF, DiNola A, Haak JR. The Journal of Chemical Physics. 1984; 81:3684–3690.
37. Jorgensen WL, Tirado-Rives J. Journal of the American Chemical Society. 1988; 110:1657–1666.

38. Teleman O, Jönsson B, Engström S. Molecular Physics: An International Journal at the Interface Between Chemistry and Physics. 1987; 60:193–203.
39. Lee JH, Labadie C, Springer CS Jr, Harbison GS. Journal of the American Chemical Society. 1993; 115:7761–7764.
40. Washburn K, Callaghan P. Physical review letters. 2006; 97:175502. [PubMed: 17155481]
41. Lang E, Lüdemann H-D. Berichte der Bunsengesellschaft für physikalische Chemie. 1980; 84:462–470.
42. Cummins PL, Bacskay GB, Hush NS, Halle B, Engström S. The Journal of chemical physics. 1985; 82:2002.
43. Lang E, Piculell L, Lüdemann H-D. The Journal of Chemical Physics: J. Chem. Phys. 1984; 81:3820–3827.
44. Bhattacharyya K, Bagchi B. The Journal of Physical Chemistry A. 2000; 104:10603–10613.
45. Nandi N, Bhattacharyya K, Bagchi B. Chemical Reviews. 2000; 100:2013–2046. [PubMed: 11749282]
46. D'Angelo M, Fioretto D, Onori G, Palmieri L, Santucci A. Phys. Rev. E. 1996; 54:993–996.
47. Datta A, Pal SK, Mandal D, Bhattacharyya K. The Journal of Physical Chemistry B. 1998; 102:6114–6117.
48. Brauns EB, Madaras ML, Coleman RS, Murphy CJ, Berg MA. Journal of the American Chemical Society. 1999; 121:11644–11649.
49. Senapati S, Chandra A. The Journal of chemical physics. 1999; 111:1223.
50. Faeder J, Ladanyi B. The Journal of Physical Chemistry B. 2000; 104:1033–1046.
51. Sun C, Mitchell O, Huang J, Boutis GS. The Journal of Physical Chemistry B. 2011; 115:13935–13942. [PubMed: 22017547]
52. Pometun MS, Gundusharma UM, Richardson JF, Wittebort RJ. Journal of the American Chemical Society. 2002; 124:2345–2351. [PubMed: 11878990]
53. Izdebski T, Akhenblit P, Jenkins JE, Yarger JL, Holland GP. Biomacromolecules. 2010; 11:168–74. [PubMed: 19894709]
54. Huang J, Sun C, Mitchell O, Ng N, Wang ZN, Boutis GS. The Journal of Chemical Physics. 2012; 136:085101. [PubMed: 22380064]
55. Li B, Alonso DO, Daggett V. Journal of Molecular Biology. 2001; 305:581–592. [PubMed: 11152614]
56. Simmons A, Ray E, Jelinski LW. Macromolecules. 1994; 27:5235–5237.
57. Asakura T, Yang M, Kawase T, Nakazawa Y. Macromolecules. 2005; 38:3356–3363.
58. Van Beek J, Hess S, Vollrath F, Meier B. Proceedings of the National Academy of Sciences. 2002; 99:10266–10271.
59. Ashida J, Ohgo K, Komatsu K, Kubota A, Asakura T. Journal of biomolecular NMR. 2003; 25:91–103. [PubMed: 12652118]
60. Keten S, Buehler MJ. Journal of the Royal Society Interface. 2010; 7:1709–1721.
61. Jenkins JE, Creager MS, Butler EB, Lewis RV, Yarger JL, Holland GP. Chemical Communications. 2010; 46:6714–6716. [PubMed: 20733981]
62. Savage KN, Gosline JM. Journal of Experimental Biology. 2008; 211:1948–1957. [PubMed: 18515725]
63. Urry DW, Trapane TL, Iqbal M, Venkatachalam CM, Prasad KU. Biochemistry. 1985; 24:5182–5189. [PubMed: 4074687]
64. Meyer DE, Chilkoti A. Biomacromolecules. 2004; 5:846–51. [PubMed: 15132671]
65. Chilkoti A, Dreher MR, Meyer DE. Advanced Drug Delivery Reviews. 2002; 54:1093–1111. [PubMed: 12384309]
66. Massodi I, Thomas E, Raucher D. Molecules. 2009; 14:1999–2015. [PubMed: 19513001]
67. MacKay AJ, Chen M, McDaniel JR, Liu W, Simnick AJ, Chilkoti A. Nature Materials. 2009; 8:993–999.
68. Herrero-Vanrell R, Rincón a. C. Alonso M, Reboto V, Molina-Martinez IT, Rodríguez-Cabello JC. Journal of Controlled Release. 2005; 102:113–22. [PubMed: 15653138]

69. Bidwell GL, Davis AN, Fokt I, Priebe W, Raucher D. Investigational New Drugs. 2007; 25:313–26. [PubMed: 17483874]

70. McDaniel JR, Callahan DJ, Chilkoti A. Advanced Drug Delivery Reviews. 2010; 62:1456–67. [PubMed: 20546809]

71. Liu W, MacKay JA, Dreher MR, Chen M, McDaniel JR, Simnick AJ, Callahan DJ, Zalutsky MR, Chilkoti A. Journal of Controlled Release. 2010; 144:2–9. [PubMed: 20117157]

72. Nettles DL, Chilkoti A, Setton LA. Advanced Drug Delivery Reviews. 2010; 62:1479–1485. [PubMed: 20385185]

73. Banki MR, Feng L, Wood DW. Nature Methods. 2005; 2:659–661. [PubMed: 16074986]

74. Megeed Z, Winters RM, Yarmush ML. Biomacromolecules. 2006; 7:999–1004. [PubMed: 16602713]

75. Jenkins JE, Creager MS, Lewis RV, Holland GP, Yarger JL. Biomacromolecules. 2010; 11:192–200. [PubMed: 20000730]

76. Jenkins JE, Creager MS, Butler EB, Lewis RV, Yarger JL, Holland GP. Chemical Communications. 2010; 46:6714–6716. [PubMed: 20733981]

77. Abragam, A. The Principles of Nuclear Magnetism. Clarendon Press; 1961.

78. Bloembergen N, Purcell EM, Pound RV. Physical Review. 1948; 73:679–712.

79. Duer, M. Introduction to solid-state NMR spectroscopy. Blackwell; 2004.

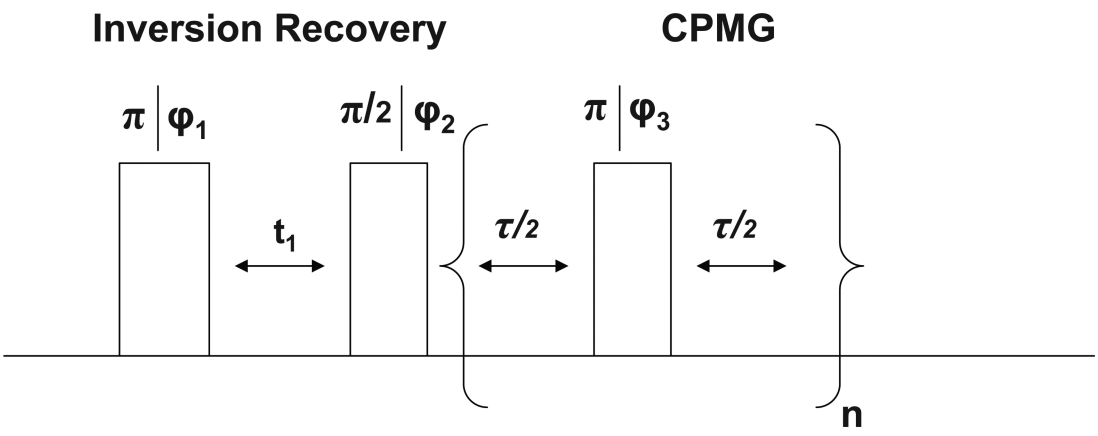

FIG. 1.

NMR pulse sequence used in the 2D T_1-T_2 correlation experiment[32]. The phase cycling was φ_1= x, –x, φ_2= x, x, –x, –x, φ_3 = y and the receiver phase was $\varphi_{Receiver}$ = x, x, –x, –x. In the experiment, the delay t_1 is varied from 5 ms to 2 s; the T_2 is measured with a CPMG train with n=6000 stroboscopically detected echo peaks[79].

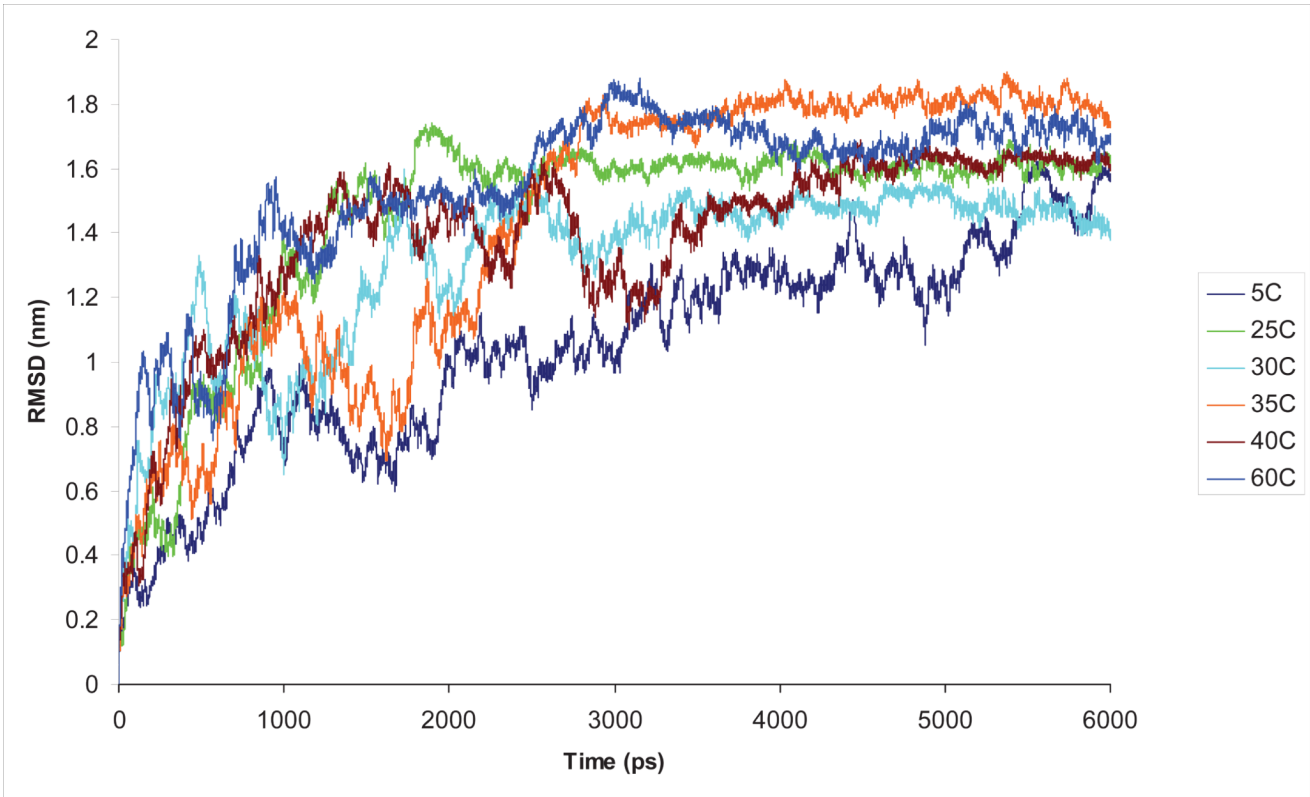

FIG. 2.

Root Mean Square Deviation (RMSD) for $(GPGSG)_5$ averaged over all C_α as a function of time for the temperatures of 5 to 60°C. As discussed in the text, the data shows the peptide equilibrates approximately after 2 ns for all temperatures. Similar results were observed in the other peptides studied, as discussed in the text.

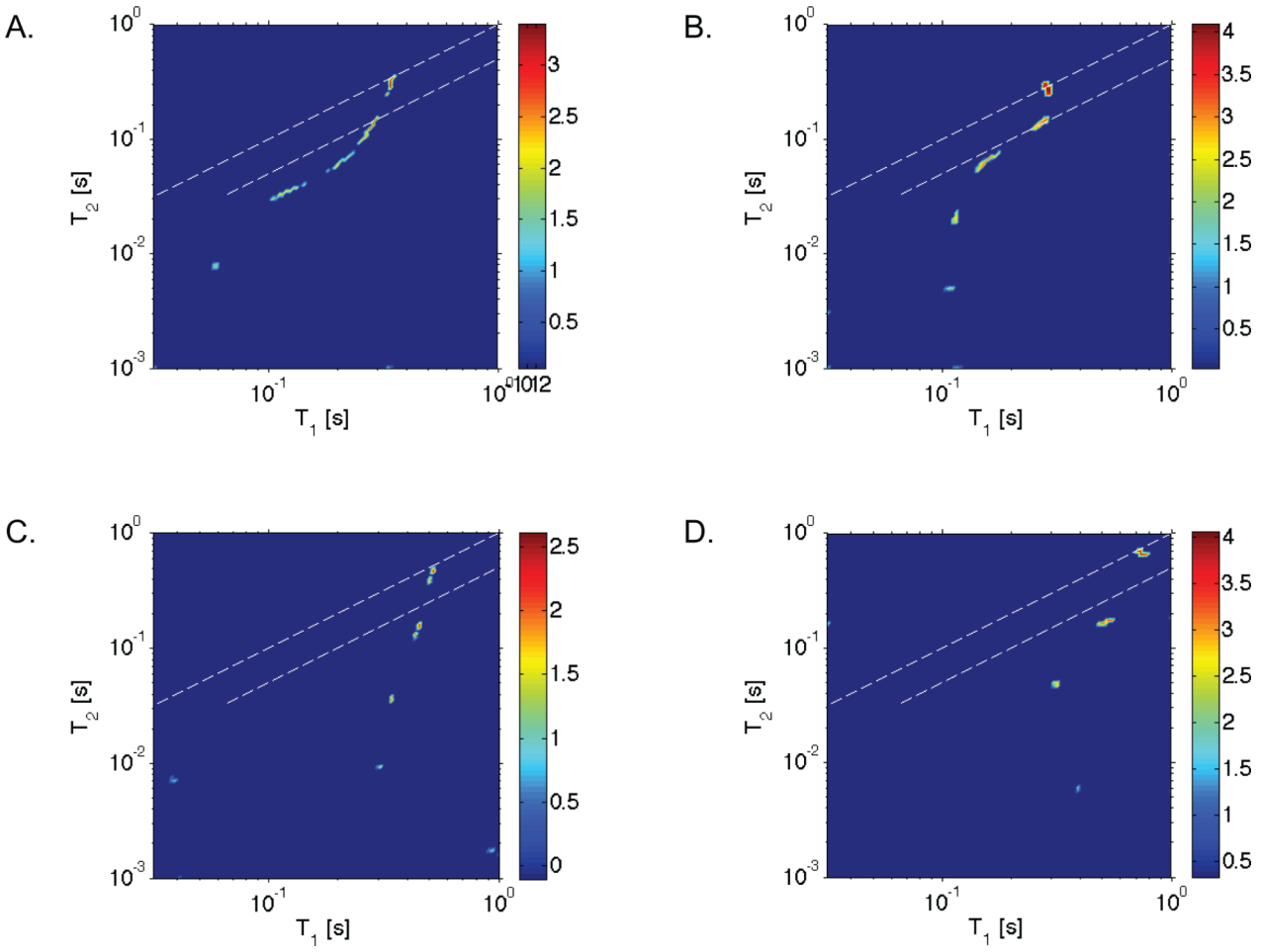

FIG. 3.

Measured T_1-T_2 ILT map of water in deuterium hydrated *N. clavipes*(A,C) and *A. aurantia*(B,D) silks at 15°C (A,B) and 50°C(C,D). Five peaks are observed corresponding to five reservoirs of water with distinguishable dynamical characteristics at low temperature and four peaks were observed at high temperatures. In the figures, the peaks with the largest T_1 and T_2 times are bulk water. The dashed lines in the figures represent a range of values where T_1 is approximately equal to T_2, and the colorbar shown represents the signal intensity on a logarithmic scale.

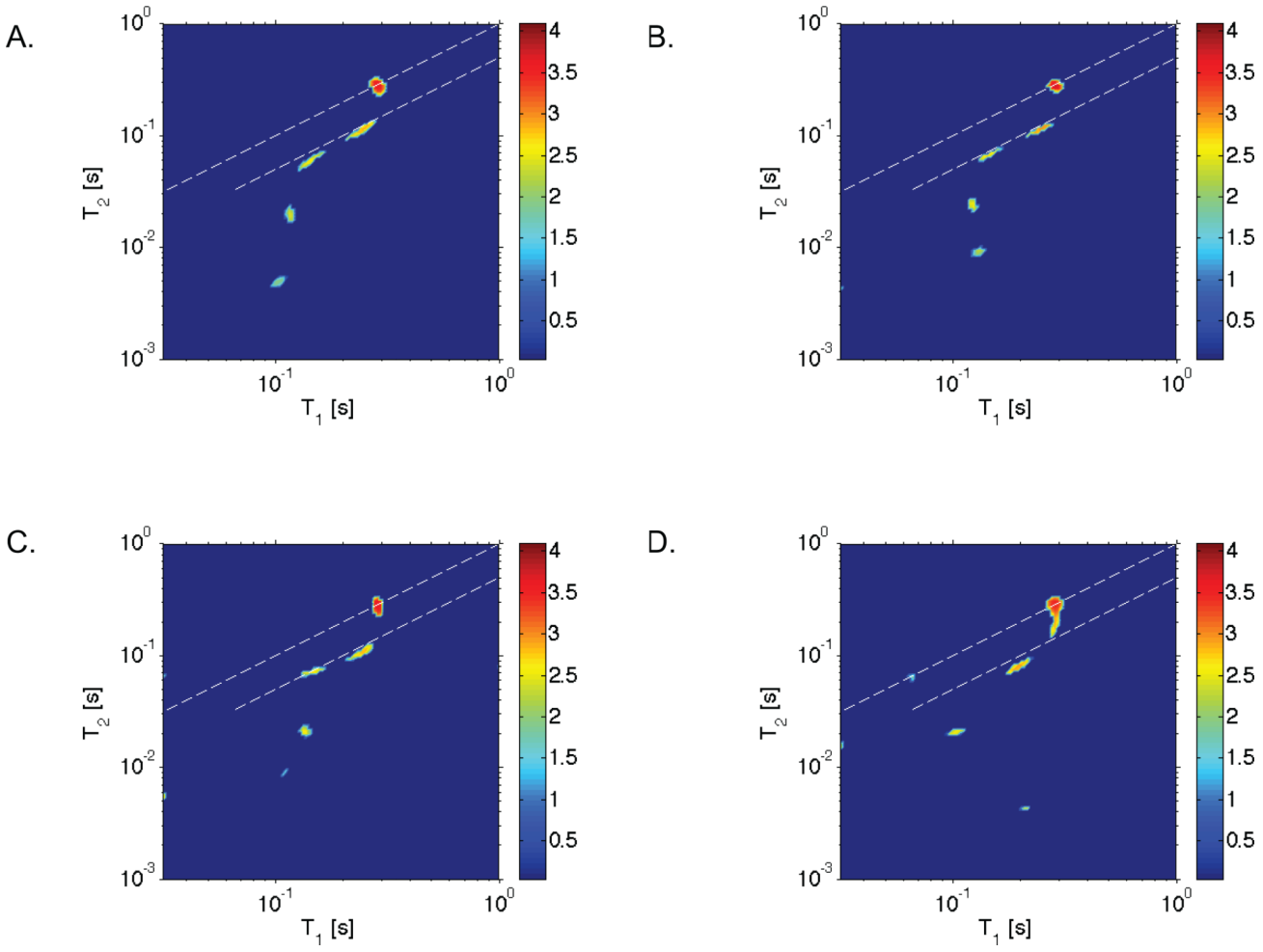

FIG. 4.

Simulated ILT maps using the experimental values from *A. aurantia* silk at 15°C (refer to Figure 3 B) with Gaussian distributed noise where the standard deviation of the noise intensity was A) set equal to that in the experiments or B) 5 times C) 7 times and D) 10 times that in the experiments. As discussed in the text, the simulations reveal that the inverse Laplace algorithm we implemented faithfully reproduces the T_1-T_2 times as well as the relative signal intensities, even in conditions where the noise is artificially set to 5 times that realized in the experiments. The experimental signal to noise in the these measurements is known to e ect the performance of the inverse Laplace algorithm we implemented, as shown elsewhere[32].

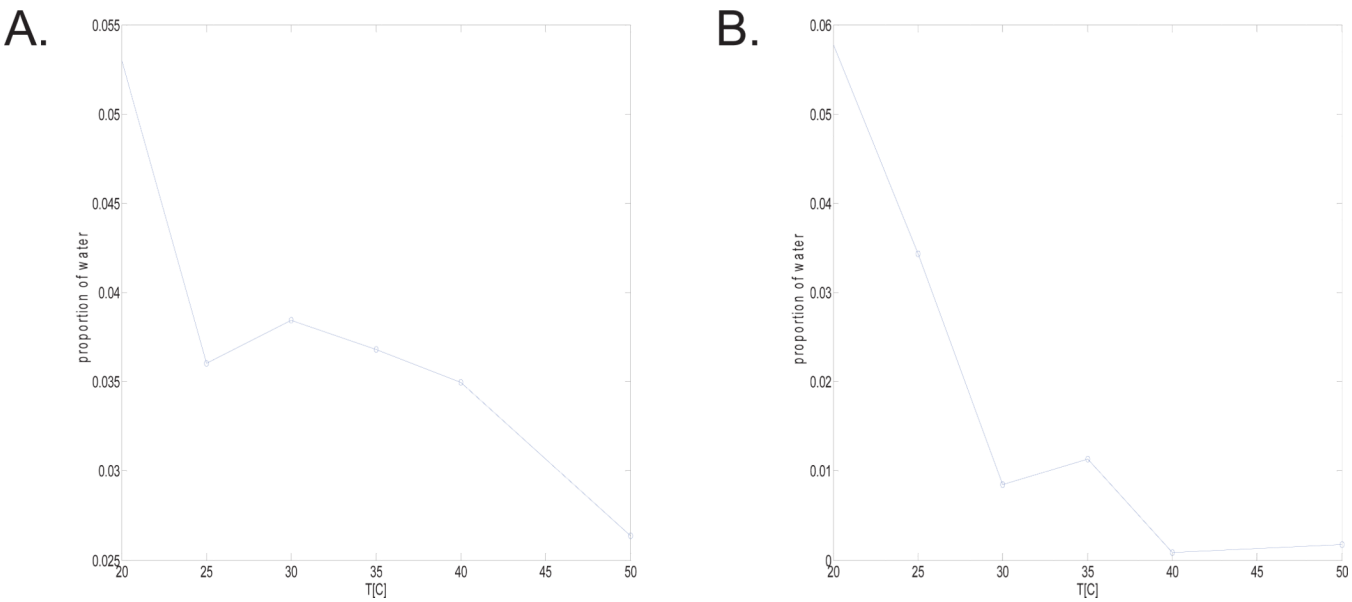

FIG. 5.

Relative population of the waters of hydration exhibiting $T_1 > T_2$ as a function of temperature in A) *N. clavipes* and B) *A. aurantia* silks. As discussed in the text, the graphs show that these components reduce in signal intensity as the temperature is increased from 20 to 50°C. A similar trend as a function of temperature was observed in the MD based studies of several short repeating motifs found in each silk sample.

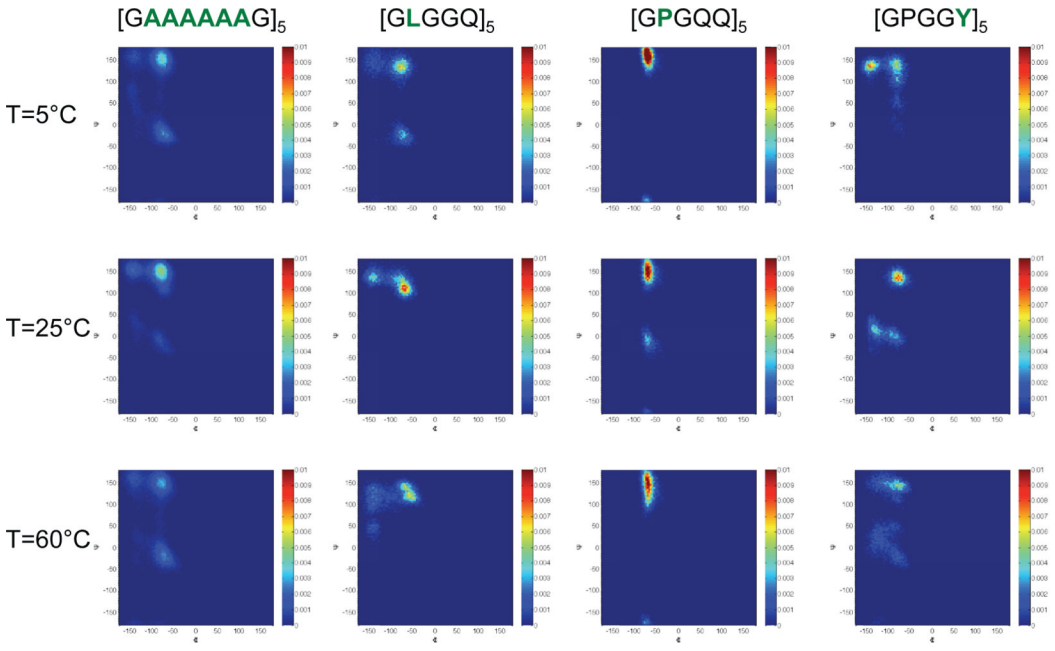

FIG. 6.

Ramachandran maps resulting from simulations of the various short peptide motifs at 5°C, 25°C and 60°C. The figure highlights the backbone conformations for alanine ($[GAAAAAAG]_5$, leucine($[GLGGQ)_5]$, proline($[GPGQQ]_5$) and tyrosine($[GPGGY_5]$). As discussed in the text, changes in temperature are observed pointing to a broadening of the dihedral angle range that is taken up by the motifs between the low and high temperatures. In the figure, the color scale denotes the number of occurrences a particular dihedral angle was measured over 1 ns of simulation time; the integrated area of the Ramachandran space was normalized to unity for ease of comparison between the temperatures.

TABLE I

Average amino acid composition of major ampullate dragline silk of various spider silks.[22]

Amino Acid	*A. argentata*	*A. aurantia*	*N. clavipes*
Gly	44.6	46.4	47.1
Ala	19.3	17.9	26.5
Pro	10.2	9.5	1.2
Ser	6.8	5.9	3.0
Tyr	5.4	4.8	3.6
Leu	1.0	1.5	4.2

TABLE II

Repeating motifs (shown in color) found in MaSp1 and MaSp2 silks from *N. clavipes* studied in the MD simulations of this work.[75]

N.clavipes
MaSp1
QGAGAAAAAAGGAGQGGYGGLGGQGAGQGGYGGLGGQGAGQGAGAAAAAAAGGAGQGGYGGLGSQGAGRGGQGAGAAAAAAGGAGQGGYGGLGSQG
AGRGGLGGQGAGAAAAAAAGGAGQGGYGGLGNQGAGRGGQGAAAAAAGGAGQGGYGGLGSQGARGGLGGQGAGAAAAAAGGAGQGGYGGLGGQ
GAGQGGYGGLGSQGAGRGGLGGQGAGAAAAAAAGGAGQGGLGGQGAGQGAGASAAAAGGAGQGGYGGLGSQGAGRGGEGAGAAAAAAGGAGQGGY
GGLGGQGAGQGGYGGLGSQGAGRGGLGGQGAGAAAAGGAGQGGLGGQGAGQGAGAAAAAAGGAGQGGYGGLGSQGAGRGGLGGQGAGAVAA
AAAGGAGQGGYGGLGSQGAGRGGQGAGAAAAAAGGAGQRGYGGLGNQGAGRGGLGGQGAGAAAAAAAGGAGQGGYGGLGNQGAGRGGQG
AAAAAGGAGQGGYGGLGSQGAGRGGQGAGAAAAAAVGAGQEGIRGQGAGQGGYGGLGSQGSGRGGLGGQGAGAAAAAAGGAGQGGLGGQGAGQGA
GAAAAAAGGVRQGGYGGLGSQGAGRGGQGAGAAAAAAGGAGQGGYGGLGGQGVGRGGLGGQGAGAAAAGGAGQGGYGGVGSGASAASAAASRLSSPQA
SSRLSSAVSNLVATGPTNSAALSSTISNVVSQIGASILVFLDVMSSFKLFSRLFLLLSRS
MaSp2
PGGYGPGQQGPGGYGPGQQGPSGPGSAAAAAAAAAAGPGGYGPGQQGPGGYGPGQQGPGRYGPGQQGPSGPGSAAAAAAGSGQQGPGGYGPRQQ
GPGGYGQGQQGPSGPGSAAAASAAASAESGQQGPGGYGPGQQGPGGYGPGQQGPGGYGPGQQGPSGPGSAAAAAAAASGPGQQGPGGYGPGQQ
GPGGYGPGQQGPSGPGSAAAAAAAASGPGQQGPGGYGPGQQGPGGYGPGQQGLSGPGSAAAAAAAGPGQQGPGGYGPGQQGPSGPGS
AAAAAAAAAGPGGYGPGQQGPGGYGPGQQGPSGAGSAAAAAAAGPGQQGLGGYGPGQQGPGGYGPGQQGPGGYGPGSASAAAAAAGPGQQ
GPGGYGPGQQGPSGPGSASAAAAAAAAAGPGGYGPGQQGPGGYAPGQQGPSGPGSASAAAAAAAAAGPGGYGPGQQGPGGYAPGQQGPSG
PGSAAAAAAAAAGPGGYGPAQQGPSGPGIAASAASAGPGGYGPAQQGPAGYGPGSAVAASAGAGSAGYGPGSQASAAASRLASPDS
GARVASAVSNLVSSGPTSSAALSSVISNAVSQIGASNPGLSGCDVLIQALLEIVSACVTILSSSSIGQVNYGAASQFAQVVGQSVLSAF

TABLE III

Repeating motifs (shown in color) found in MaSp1 and MaSp2 silks from *A. aurantia*[76] studied in the MD simulations of this work.

A.aurantia
MaSp1
AGQGGAGAAAAAAAAGGAGGAGRGGLGAGGAGQGYGSGLGGQGGAGGGAAAAAAAAAGGQGGQGGYGGLGSQGAGQGGYGAGQ
GGAGAAAAAAAAGGAGGAGRGGLGAGGAGQGYGSGLGGQGGAGQGGAAAAAAAAGGQGGQGGYGGLGSQGAGQGGAGRGAAAA
AAAAGGQGGRGGYGGLGSQGAGQGGYGAGQGGAGAAAAAAAAGGAGEGGLGAGGAGQGYGSGLGGQGGAGQGG
AAAAAAAAGGQGGHGGYGGLGSQGAGQGGAGRGAAAAAAAAGGQGGQGGYGGLGSQGAGQGGYGAGQGGAAAAA
AAAAAGGAGGAGRGELGAGGAGQGYGXGLGGQGGAGQRGAASVAALAGGQGGQGGFGGFSSQGAGQGAYGGGAYSGQGAAASVSAASAAASRLS
SPGAASRVSSAVTSLVSSGGPTNPAALSNTISXVVSQISE
MaSp2
PGGAGQQGPGGQGPYGPGAAAAAAAAGGYGPGAGQQGPXGAGQQGPGSQGPGGAGQQGPGGQGPYGPGAAAAAAAVGGYGPGAGQQ
GPGSQGPGSGGQQGPGGQGPYGPSAAAAAAAAGGYGPGAGQQGPGSQGPGSGGQQGPGGLGPYGPSAAAAAAAAGGYGPGAGQQGPGSQGPGSG
GQQRPGGLGPYGPSAAAAAAAAGGYGPGAGQQGPGSQGPGSGGQQRPGGLGPYGPSAAAAAAAAGGYGPGAGQQGPGSQAPVASAAASRLSSPQA
SSRVSSAVSTLVSSGPTNPAALSNAISSVVSQVSASNPGLSGCDVLVQALLELVSALVHILGSSSIGQINYAAS

TABLE IV

Molecular dynamics based findings for $[GPGSG]_5$ (top) and $[GPGSQ]_5$ (bottom) from 5°C to 60°C in *A. aurantia* (MaSp2) silk

Temp (°C)	Rg (nm)[A]	SASA (nm^2)[B]	Non Polar SASA (nm^2)[B]	Side-Chain Contacts[C]	Number of Water Molecules[D]	Peptide - Peptide H Bonds[E]	Peptide - Water H Bonds[E]
5	0.88 ± 0.09	19.0 ± 0.97	10.1 ± 0.63	271.7 ± 21.3	12257.3 ± 566.2	4.50 ± 1.21	52.0 ± 3.60
25	0.76 ± 0.05	18.4 ± 0.71	9.90 ± 0.43	274.8 ± 15.4	11611.3 ± 503.6	4.24 ± 1.38	49.6 ± 3.90
30	0.70 ± 0.03	16.5 ± 0.74	9.25 ± 0.36	332.5 ± 13.6	10237.0 ± 434.2	8.99 ± 2.03	40.7 ± 4.08
35	0.79 ± 0.02	17.7 ± 0.56	9.85 ± 0.34	292.1 ± 9.15	11037.0 ± 366.1	7.67 ± 1.87	43.3 ± 4.03
40	0.75 ± 0.03	16.7 ± 0.47	9.22 ± 0.33	326.7 ± 11.6	10428.5 ± 278.4	7.18 ± 1.43	43.2 ± 3.66
60	0.73 ± 0.03	17.0 ± 0.55	9.51 ± 0.36	306.7 ± 10.2	10311.8 ± 374.0	7.48 ± 1.32	42.5 ± 3.72

Temp (°C)	Rg (nm)[A]	SASA (nm^2)[B]	Non Polar SASA (nm^2)[B]	Side-Chain Contacts[C]	Number of Water Molecules[D]	Peptide - Peptide H Bonds[E]	Peptide - Water H Bonds[E]
5	1.64 ± 0.09	24.4 ± 0.66	11.4 ± 0.31	260.4 ± 16.4	15652.9 ± 438.3	2.17 ± 1.45	71.8 ± 4.55
25	1.67 ± 0.09	23.0 ± 0.63	11.2 ± 0.30	272.8 ± 11.9	14696.4 ± 423.4	4.71 ± 1.30	65.0 ± 4.42
30	0.85 ± 0.07	21.6 ± 0.85	9.85 ± 0.54	322.1 ± 19.8	13664.9 ± 609.5	4.32 ± 1.36	64.7 ± 4.32
35	0.90 ± 0.02	19.7 ± 0.49	9.55 ± 0.35	368.5 ± 10.5	12304.9 ± 330.3	9.27 ± 1.72	53.6 ± 4.21
40	0.82 ± 0.03	20.3 ± 0.81	10.0 ± 0.45	333.4 ± 16.7	12775.3 ± 496.2	6.58 ± 1.79	58.3 ± 4.64
60	0.85 ± 0.06	20.5 ± 0.85	9.68 ± 0.46	335.2 ± 23.2	12291.5 ± 609.7	6.37 ± 1.78	56.6 ± 5.04

The errors shown in the table were determined by the standard deviation of the fluctuations observed over the 2 ns of data used in the analysis, as discussed in the text.

[A] radius of gyration averaged over all C_α

[B] solvent accessible surface area (SASA) was computed with the minimum distance set to 0.14nm

[C] side-chain contacts were counted when two neighboring aliphatic carbon atoms from neighboring residues were within 0.65nm of each other

[D] number of water molecules were counted when a water molecule is within 0.6nm of any protein atoms, and (E) hydrogen bonds are defined as when the hydrogen and the acceptor atoms are within 0.35nm.

[E] hydrogen bonds are defined as when the hydrogen and the acceptor atoms are within 0.35nm.

TABLE V

Molecular dynamics based findings for $[GYGSG]_5$ (top) and $[GLGSQ]_5$ (bottom) from 5°C to 60°C in *A. aurantia* (MaSp1) silk (the repeating motif $[GLGSQ]_5$ also appears in *N. Clavipes* MaSp1)

Temp (°C)	Rg (nm)[A]	SASA (nm^2)[B]	Non Polar SASA (nm^2)[B]	Side-Chain Contacts[C]	Number of Water Molecules[D]	Peptide - Peptide H Bonds[E]	Peptide - Water H Bonds[E]
5	1.27 ± 0.14	25.7 ± 0.90	13.2 ± 0.60	228.8 ± 10.9	16039.4 ± 467.6	0.43 ± 0.60	75.8 ± 4.48
25	0.87 ± 0.04	18.3 ± 0.64	9.75 ± 0.35	354.9 ± 13.8	11854.2 ± 380.1	8.08 ± 1.39	56.6 ± 4.21
30	0.76 ± 0.02	19.2 ± 0.61	10.2 ± 0.36	346.4 ± 11.7	12461.3 ± 398.6	4.53 ± 1.14	61.8 ± 4.07
35	0.77 ± 0.05	18.9 ± 0.52	10.3 ± 0.37	340.1 ± 10.8	11914.2 ± 331.9	8.33 ± 1.89	55.0 ± 4.29
40	0.90 ± 0.06	21.3 ± 0.74	10.9 ± 0.57	313.0 ± 14.4	13236.9 ± 431.2	3.44 ± 1.51	64.5 ± 4.51
60	0.72 ± 0.02	17.4 ± 0.58	9.69 ± 0.44	377.3 ± 11.7	10812.1 ± 378.2	9.96 ± 1.96	49.4 ± 4.04

Temp (°C)	Rg (nm)[A]	SASA (nm^2)[B]	Non Polar SASA (nm^2)[B]	Side-Chain Contacts[C]	Number of Water Molecules[D]	Peptide - Peptide H Bonds[E]	Peptide - Water H Bonds[E]
5	1.21 ± 0.05	25.9 ± 0.60	13.4 ± 0.35	257.6 ± 12.1	17174.6 ± 354.9	4.28 ± 1.24	74.5 ± 4.20
25	0.81 ± 0.05	21.0 ± 0.84	10.9 ± 0.48	331.1 ± 12.1	14177.2 ± 494.9	7.65 ± 1.75	62.3 ± 4.46
30	0.96 ± 0.04	21.3 ± 0.57	11.4 ± 0.46	316.8 ± 13.1	14274.2 ± 401.2	7.45 ± 2.20	61.9 ± 5.06
35	1.15 ± 0.11	23.2 ± 1.08	12.3 ± 0.59	259.8 ± 11.4	15311.1 ± 589.2	5.92 ± 2.36	65.1 ± 5.04
40	0.79 ± 0.05	20.3 ± 1.07	10.3 ± 0.56	306.4 ± 19.9	13473.2 ± 670.2	5.57 ± 1.53	60.3 ± 5.09
60	0.74 ± 0.01	20.2 ± 0.72	10.9 ± 0.34	330.0 ± 11.0	12991.5 ± 456.8	8.63 ± 2.08	54.0 ± 4.39

The errors shown in the table were determined by the standard deviation of the fluctuations observed over the 2 ns of data used in the analysis, as discussed in the text.

[A] radius of gyration averaged over all C_α

[B] solvent accessible surface area (SASA) was computed with the minimum distance set to 0.14nm

[C] side-chain contacts were counted when two neighboring aliphatic carbon atoms from neighboring residues were within 0.65nm of each other

[D] number of water molecules were counted when a water molecule is within 0.6nm of any protein atoms

[E] hydrogen bonds are defined as when the hydrogen and the acceptor atoms are within 0.35nm.

TABLE VI

Molecular dynamics based findings for $[GLGGQ]_5$ (top) and $[GAAAAAAG]_5$ (bottom) from 5°C to 60°C in *N. clavipes* (MaSp1) silk (the motif $[GLGGQ]_5$ also appears in the MaSp1 sequence of *A. aurantia*)

Temp (°C)	Rg (nm)[A]	SASA (nm^2)[B]	Non Polar SASA (nm^2)[B]	Side-Chain Contacts[C]	Number of Water Molecules[D]	Peptide - Peptide H Bonds[E]	Peptide - Water H Bonds[E]
5	1.24 ± 0.12	24.0 ± 0.64	11.6 ± 0.41	248.5 ± 12.8	15653.7 ± 393.0	1.93 ± 0.86	69.2 ± 4.19
25	0.69 ± 0.02	17.3 ± 0.74	9.03 ± 0.39	372.9 ± 14.3	11573.5 ± 521.6	9.12 ± 1.84	48.7 ± 4.84
30	0.72 ± 0.03	18.3 ± 0.78	9.20 ± 0.46	381.2 ± 14.5	12036.9 ± 504.2	8.31 ± 1.69	51.1 ± 4.21
35	0.94 ± 0.08	21.3 ± 0.89	11.1 ± 0.53	291.6 ± 22.8	13750.3 ± 523.6	6.58 ± 1.88	56.3 ± 5.08
40	0.80 ± 0.03	18.5 ± 0.78	9.23 ± 0.48	370.2 ± 18.7	11958.9 ± 460.0	6.99 ± 1.56	51.6 ± 4.42
60	0.68 ± 0.02	17.8 ± 0.51	9.41 ± 0.35	376.9 ± 12.7	11306.5 ± 388.0	9.41 ± 1.86	46.1 ± 4.21

Temp (°C)	Rg (nm)[A]	SASA (nm^2)[B]	Non Polar SASA (nm^2)[B]	Side-Chain Contacts[C]	Number of Water Molecules[D]	Peptide - Peptide H Bonds[E]	Peptide - Water H Bonds[E]
5	2.44 ± 0.10	32.6 ± 0.56	19.7 ± 0.44	387.2 ± 10.9	21032.4 ± 423.6	3.87 ± 1.31	82.1 ± 4.62
25	0.88 ± 0.03	25.4 ± 0.80	15.7 ± 0.57	509.2 ± 15.4	17061.2 ± 511.2	9.04 ± 1.72	68.6 ± 4.49
30	0.87 ± 0.02	24.5 ± 0.69	15.0 ± 0.57	540.6 ± 14.4	16100.4 ± 499.0	8.20 ± 1.84	63.2 ± 4.52
35	2.76 ± 0.10	29.8 ± 1.84	18.3 ± 0.10	428.8 ± 32.5	19146.5 ± 975.9	5.87 ± 1.75	73.9 ± 5.61
40	1.22 ± 0.07	28.0 ± 0.79	17.0 ± 0.48	464.4 ± 15.7	17825.1 ± 498.1	5.61 ± 1.57	69.9 ± 4.67
60	1.21 ± 0.09	27.8 ± 0.92	17.1 ± 0.54	466.7 ± 16.4	17209.0 ± 569.5	6.65 ± 1.76	65.3 ± 5.10

The errors shown in the table were determined by the standard deviation of the fluctuations observed over the 2 ns of data used in the analysis, as discussed in the text.

[A] radius of gyration averaged over all C_α

[B] solvent accessible surface area (SASA) was computed with the minimum distance set to 0.14nm

[C] side-chain contacts were counted when two neighboring aliphatic carbon atoms from neighboring residues were within 0.65nm of each other

[D] number of water molecules were counted when a water molecule is within 0.6nm of any protein atoms

[E] hydrogen bonds are defined as when the hydrogen and the acceptor atoms are within 0.35nm.

TABLE VII

Molecular dynamics based findings for $[GPGQQ]_5$ (top) and $[GPGGY]_5$ (bottom) from 5°C to 60°C in *N. clavipes* (MaSp2) silk

Temp (°C)	Rg (nm)[A]	SASA (nm^2)[B]	Non Polar SASA (nm^2)[B]	Side-Chain Contacts[C]	Number of Water Molecules[D]	Peptide - Peptide H Bonds[E]	Peptide - Water H Bonds[E]
5	1.55 ± 0.10	25.7 ± 0.66	10.5 ± 0.41	259.7 ± 13.9	16850.3 ± 450.3	1.60 ± 1.13	81.5 ± 4.84
25	0.88 ± 0.08	20.3 ± 0.64	8.63 ± 0.39	367.8 ± 18.3	13742.6 ± 570.8	5.66 ± 2.10	66.7 ± 5.56
30	0.79 ± 0.01	19.1 ± 0.46	8.33 ± 0.35	364.7 ± 10.7	12965.5 ± 361.8	8.49 ± 1.72	61.3 ± 4.49
35	0.91 ± 0.02	20.6 ± 0.57	8.68 ± 0.28	333.5 ± 15.2	13736.8 ± 407.3	7.13 ± 1.71	64.2 ± 4.58
40	1.00 ± 0.03	21.4 ± 0.57	8.75 ± 0.36	315.5 ± 11.6	14093.3 ± 398.5	5.09 ± 1.29	67.5 ± 4.69
60	0.95 ± 0.10	21.4 ± 0.81	9.07 ± 0.36	327.5 ± 13.3	13685.1 ± 484.5	5.75 ± 2.08	64.2 ± 5.41

Temp (°C)	Rg (nm)[A]	SASA (nm^2)[B]	Non Polar SASA (nm^2)[B]	Side-Chain Contacts[C]	Number of Water Molecules[D]	Peptide - Peptide H Bonds[E]	Peptide - Water H Bonds[E]
5	1.16 ± 0.05	21.2 ± 0.43	13.2 ± 0.36	377.5 ± 10.4	14073.8 ± 331.3	3.85 ± 1.13	52.1 ± 3.42
25	0.68 ± 0.01	17.3 ± 0.49	10.6 ± 0.35	462.7 ± 18.1	11570.6 ± 343.3	6.91 ± 1.20	44.3 ± 3.18
30	1.97 ± 0.04	23.1 ± 0.60	13.9 ± 0.50	364.3 ± 15.4	14778.2 ± 381.5	2.32 ± 0.78	54.4 ± 3.89
35	0.77 ± 0.02	19.5 ± 0.53	12.1 ± 0.41	457.1 ± 25.7	12649.5 ± 383.1	5.21 ± 1.25	47.4 ± 3.90
40	0.79 ± 0.03	18.3 ± 0.54	11.3 ± 0.42	485.8 ± 31.4	11852.5 ± 412.5	5.91 ± 1.57	43.2 ± 3.95
60	0.68 ± 0.02	18.1 ± 0.53	11.1 ± 0.39	512.5 ± 19.9	11202.7 ± 402.6	6.40 ± 1.44	40.9 ± 3.85

The errors shown in the table were determined by the standard deviation of the fluctuations observed over the 2 ns of data used in the analysis, as discussed in the text.

[A] radius of gyration averaged over all C_α

[B] solvent accessible surface area (SASA) was computed with the minimum distance set to 0.14nm

[C] side-chain contacts were counted when two neighboring aliphatic carbon atoms from neighboring residues were within 0.65nm of each other

[D] number of water molecules were counted when a water molecule is within 0.6nm of any protein atoms

[E] hydrogen bonds are defined as when the hydrogen and the acceptor atoms are within 0.35nm.

TABLE VIII

Molecular dynamics based findings for $[GPSG]_5$ (top) and $[GPSGPGS]_5$ (bottom) from 5°C to 60°C in *N. clavipes* (MaSp2) silk

Temp (°C)	Rg (nm)[A]	SASA (nm^2)[B]	Non Polar SASA (nm^2)[B]	Side-Chain Contacts[C]	Number of Water Molecules[D]	Peptide - Peptide H Bonds[E]	Peptide - Water H Bonds[E]
5	0.78 ± 0.04	16.4 ± 0.50	8.81 ± 0.24	210.1 ± 8.59	11012.4 ± 322.2	1.61 ± 1.01	46.2 ± 3.67
25	0.90 ± 0.03	15.1 ± 0.41	8.44 ± 0.31	241.2 ± 7.90	10196.1 ± 307.7	4.40 ± 1.16	38.8 ± 3.50
30	0.66 ± 0.02	13.5 ± 0.49	7.24 ± 0.34	264.3 ± 11.5	9137.8 ± 351.9	3.70 ± 1.41	38.5 ± 3.59
35	1.00 ± 0.06	16.6 ± 0.69	9.18 ± 0.45	208.9 ± 17.5	10654.7 ± 438.4	3.36 ± 1.39	41.1 ± 3.59
40	0.66 ± 0.04	14.1 ± 0.57	7.88 ± 0.30	264.4 ± 11.5	9200.0 ± 381.2	5.65 ± 1.65	35.6 ± 3.60
60	0.69 ± 0.02	14.6 ± 0.45	7.92 ± 0.28	251.4 ± 10.2	9275.9 ± 345.9	2.69 ± 1.50	38.2 ± 3.82

Temp (°C)	Rg (nm)[A]	SASA (nm^2)[B]	Non Polar SASA (nm^2)[B]	Side-Chain Contacts[C]	Number of Water Molecules[D]	Peptide - Peptide H Bonds[E]	Peptide - Water H Bonds[E]
5	1.07 ± 0.03	27.9 ± 0.53	15.3 ± 0.39	414.6 ± 10.4	19284.7 ± 408.1	2.99 ± 0.73	80.9 ± 4.39
25	0.98 ± 0.03	26.1 ± 1.12	14.8 ± 0.70	465.1 ± 27.2	17800.0 ± 662.8	5.37 ± 1.77	72.5 ± 5.06
30	0.95 ± 0.03	24.0 ± 0.71	13.6 ± 0.45	493.3 ± 13.5	16643.4 ± 487.9	5.71 ± 1.53	68.1 ± 4.91
35	0.84 ± 0.02	22.2 ± 0.44	13.4 ± 0.33	524.2 ± 11.1	15355.4 ± 373.2	11.1 ± 1.57	60.2 ± 3.84
40	0.86 ± 0.01	22.6 ± 0.58	12.8 ± 0.35	558.8 ± 12.8	15678.0 ± 410.2	5.93 ± 1.36	67.5 ± 4.22
60	0.99 ± 0.04	24.4 ± 1.53	14.0 ± 0.77	475.7 ± 30.6	16068.1 ± 894.0	7.48 ± 2.09	62.3 ± 5.72

The errors shown in the table were determined by the standard deviation of the fluctuations observed over the 2 ns of data used in the analysis, as discussed in the text.

[A] radius of gyration averaged over all C_α

[B] solvent accessible surface area (SASA) was computed with the minimum distance set to 0.14nm

[C] side-chain contacts were counted when two neighboring aliphatic carbon atoms from neighboring residues were within 0.65nm of each other

[D] number of water molecules were counted when a water molecule is within 0.6nm of any protein atoms

[E] hydrogen bonds are defined as when the hydrogen and the acceptor atoms are within 0.35nm.

TABLE IX

Relaxation times for the components with $T_1 > T_2$ in the T_1-T_2 2D experiment performed on *N. clavipes* silk.

Temp [°C]	T1 [s]	T2 [s]	$\tau_c \times 10^{-9}$ [s]	$4\pi^2 C_{Q_{eff}}^2 \times 10^{10} [s^{-2}]$
5	.04409 ± .0014	.00392 ± .0003	18.4 ± 1.34	10.86 ± 1.02
15	.05849 ± .0023	.00785 ± .0007	14.2 ± 1.25	6.51 ± 0.71
20	.04923 ± .0032	.00784 ± .0006	12.7 ± 1.25	7.05 ± 0.96
25	N/A	N/A	N/A	N/A
30	N/A	N/A	N/A	N/A
35	N/A	N/A	N/A	N/A
40	N/A	N/A	N/A	N/A
50	N/A	N/A	N/A	N/A

Temp [°C]	T1 [s]	T2 [s]	$\tau_c \times 10^{-9}$ [s]	$4\pi^2 C_{Q_{eff}}^2 \times 10^{10} [s^{-2}]$
5	.05251 ± .0025	.01645 ± .0004	7.45 ± 1.10	4.50 ± 0.57
15	.12174 ± .0020	.03575 ± .0065	7.89 ± 1.62	2.01 ± 0.27
20	.10915 ± .0022	.03073 ± .0036	8.21 ± 1.08	2.30 ± 0.23
25	.11742 ± .0020	.02663 ± .0030	9.82 ± 1.08	2.42 ± 0.23
30	.08661 ± .0024	.02077 ± .0018	9.38 ± 0.93	3.17 ± 0.29
35	.07325 ± .0034	.01462 ± .0009	10.8 ± 0.91	4.16 ± 0.44
40	.07852 ± .0042	.01223 ± .0007	12.9 ± 1.03	4.48 ± 0.49
50	.30243 ± .0015	.00933 ± .0005	33.1 ± 1.72	3.05 ± 0.21

Temp [°C]	T1 [s]	T2 [s]	$\tau_c \times 10^{-9}$ [s]	$4\pi^2 C_{Q_{eff}}^2 \times 10^{10} [s^{-2}]$
5	.14679 ± .0119	.04520 ± .0011	7.57 ± 1.27	1.62 ± 0.27
15	.21169 ± .0040	.06527 ± .0139	7.54 ± 1.89	1.12 ± 0.17
20	.20545 ± .0054	.05064 ± .0060	9.19 ± 1.18	1.32 ± 0.15
25	.20439 ± .0034	.04086 ± .0040	10.8 ± 0.98	1.49 ± 0.13
30	.25872 ± .0047	.04663 ± .0050	11.7 ± 1.10	1.26 ± 0.11
35	.26192 ± .0093	.04375 ± .0043	12.3 ± 1.23	1.29 ± 0.14
40	.29331 ± .0064	.04222 ± .0057	13.6 ± 1.57	1.25 ± 0.14
50	.33983 ± .0075	.03655 ± .0027	16.4 ± 1.01	1.27 ± 0.10

The tables also highlight the correlation time τ_C and constant $C_{Q_{eff}}$ as a function of temperature.[77] As discussed in the text, the measured correlation times are significantly larger than that of free water (~5 ps at room temperature)[78].

TABLE X

Relaxation times for the components with $T_1 > T_2$ in the T_1-T_2 2D experiment performed on *A. aurantia* silk.

Temp [°C]	T1 [s]	T2 [s]	$\tau_c \times 10^{-9}$ [s]	$4\pi^2 C_{Q_{eff}}^2 \times 10^{10} [s^{-2}]$
5	.10797 ± .0064	.00500 ± .0003	26.6 ± 1.72	6.26 ± 0.71
15	.16008 ± .0061	.00851 ± .0013	24.7 ± 2.82	3.94 ± 0.55
20	.14969 ± .0064	.00969 ± .0008	22.1 ± 1.67	3.79 ± 0.41
25	.19571 ± .0111	.00534 ± .0003	35.3 ± 2.13	4.54 ± 0.50
30	N/A	N/A	N/A	N/A
35	.20546 ± .0084	.00266 ± .0001	52.0 ± 2.49	6.32 ± 0.54
40	N/A	N/A	N/A	N/A
50	N/A	N/A	N/A	N/A

Temp [°C]	T1 [s]	T2 [s]	$\tau_c \times 10^{-9}$ [s]	$4\pi^2 C_{Q_{eff}}^2 \times 10^{10} [s^{-2}]$
5	.11415 ± .0044	.02098 ± .0032	11.5 ± 1.72	2.81 ± 0.42
15	.17859 ± .0073	.17859 ± .0087	10.9 ± 2.75	1.72 ± 0.37
20	.20411 ± .0083	.04699 ± .0086	9.70 ± 1.94	1.38 ± 0.24
25	.21991 ± .0098	.03969 ± .0096	11.6 ± 2.82	1.47 ± 0.32
30	.24590 ± .0106	.01943 ± .0017	19.7 ± 1.59	2.07 ± 0.23
35	.24562 ± .0083	.02575 ± .0017	16.6 ± 1.20	1.78 ± 0.17
40	.24855 ± .0055	.01076 ± .0005	27.6 ± 1.10	2.82 ± 0.17
50	.39090 ± .0095	.00595 ± .0005	47.8 ± 2.18	3.06 ± 0.21

Temp [°C]	T1 [s]	T2 [s]	$\tau_c \times 10^{-9}$ [s]	$4\pi^2 C_{Q_{eff}}^2 \times 10^{10} [s^{-2}]$
5	.16054 ± .0089	.06553 ± .0143	5.66 ± 2.03	1.27 ± 0.24
15	.20963 ± .0030	.07735 ± .0190	6.32 ± 2.40	1.03 ± 0.17
20	.29186 ± .0080	.11745 ± .0263	5.76 ± 1.89	0.71 ± 0.09
25	.27553 ± .0109	.09885 ± .0243	6.52 ± 2.26	0.80 ± 0.14
30	.26235 ± .0093	.06864 ± .0097	8.72 ± 1.45	1.00 ± 0.14
35	.29548 ± .0156	.07884 ± .0107	8.60 ± 1.45	0.88 ± 0.13
40	.29080 ± .0110	.06237 ± .0050	10.2 ± 0.98	1.00 ± 0.11
50	.31266 ± .0111	.04821 ± .0035	13.0 ± 1.01	1.13 ± 0.11

The tables also highlight the correlation time τ_C and constant $C_{Q_{eff}}$ as a function of temperature.[77]